LM-00K074
October 31, 2000

Effect of Pressure with Wall Heating in Annular Two-Phase Flow

R. Kumar, T.A. Trabold

Effect of Pressure with Wall Heating in Annular Two-Phase Flow

Ranganathan Kumar and Thomas A. Trabold
Lockheed Martin Corporation
Schenectady, NY 12301

ABSTRACT

The local distributions of void fraction, interfacial frequency and velocity have been measured in annular flow of R-134a through a wall-heated, high aspect ratio duct. High aspect ratio ducts provide superior optical access to tubes or irregular geometries. This work expands upon earlier experiments conducted with adiabatic flows in the same test section. Use of thin, transparent heater films on quartz windows provided sufficient electrical power capacity to produce the full range of two-phase conditions of interest. With wall vapor generation, the system pressure was varied from 0.9 to 2.4 MPa, thus allowing the investigation of flows with liquid-to-vapor density ratios covering the range of about 7 to 27, far less than studied in air-water and similar systems. There is evidence that for a given cross-sectional average void fraction, the local phase distributions can be different depending on whether the vapor phase is generated at the wall, or upstream of the test section inlet. In wall-heated flows, local void fraction profiles measured across both the wide and narrow test section dimensions illustrate the profound effect that pressure has on the local flow structure; notably, increasing pressure appears to thin the wall-bounded liquid films and redistribute liquid toward the edges of the test section. This general trend is also manifested in the distributions of mean droplet diameter and interfacial area density, which are inferred from local measurements of void fraction, droplet frequency and velocity. At high pressure, the interfacial area density is increased due to the significant enhancement in droplet concentration.

Nomenclature

a_i	Interfacial area density
d	Diameter, μm
f_d	Frequency of droplets, 1/sec
G	Mass flux, $kg/m^2/hr$
L	Length, mm
t	Duct thickness, mm
V	Average velocity, m/sec
V_d	Droplet velocity, m/sec
V_w	Wave velocity, m/sec
w	Mass rate of flow, kg/hr
W	Width, m
x	Quality
X	Axial dimension, m
y, Y	Thickness dimension, m
z, Z	Transverse dimension, m

Subscripts and superscripts

d	Droplet
g	Vapor
l	Liquid

Symbols

α	Void fraction
ρ	Density

Introduction

Annular two-phase flow is an area of active research because of its practical importance in a wide variety of applications in the chemical process and energy industries. From a scientific standpoint, annular flow is a particularly challenging phenomenon, because of the separation of the liquid phase between the wall-bounded film and dispersed droplets in the central gas core. The complication of phase separation in annular flow leads to the need for more sophisticated analyses and computations. The literature contains plenty of adiabatic tests in air-water. However, because of the attendant reliance on mathematical modeling, detailed experimental data in wall-heated high-pressure annular flow are required. The physical mechanisms and the physical models that describe the complex interactions that occur in annular flow have been discussed by Hewitt and Hall-Taylor [1] and Azzopardi [2]. Important contributions have also been made in the area of entrainment, deposition, interfacial shear and droplet size modeling in annular flow by Hanratty and co-workers [3-5], and by Kataoka and co-workers [6,7]. These and numerous other papers in annular flow modeling and measurements have been referenced elsewhere [2].

Much of the data in the literature have been obtained in circular tubes. High aspect ratio non-circular ducts have been used in many applications including compact heat exchangers. While presenting a clear optical access for fundamental experimentation, these geometries also present unique problems. Since the liquid film at the edge has been known to be much thicker than that at the flat side, the droplet breakup mechanism is non-isotropic, giving rise to three-dimensional topography in narrow ducts. Our earlier paper [8] provided an introduction to the measurement methods and database in adiabatic annular flow, and presented void fraction and droplet velocity distributions at 2.4 MPa in a narrow duct. These data from the hot-film anemometer were further analyzed to obtain the turbulence intensity [9], which was shown to increase with increasing droplet diameter. We also presented new measurements in adiabatic flow [10] to illustrate the effect of pressure on flows with low surface tension and low liquid-to-vapor density ratio. The measurements from these specifically designed experiments at high pressures were used to validate the integrated effects of the annular flow models in a two-dimensional three-field

formulation [11].

In our earlier work [8-10], the adiabatic annular flow was generated upstream of the test section to produce a desired cross-sectional average void fraction. This methodology is consistent with the majority of the work reported in the literature, in which a two-phase mixture is introduced at the inlet, and the flow is considered to be fully developed after being transported over some entrance length. There is little evidence in the literature that the local structure of the phase distribution produced by this method is similar to that created by an incremental production of the vapor phase by wall heating. For the design of heated two-phase flow systems, it is important to understand if an adiabatic flow has the same basic structure as a heated flow, even if the bulk flow conditions at a given cross-section are equivalent. This question is particularly relevant in connection with computational analyses in which mathematical models for heated systems are based upon data obtained in adiabatic experiments.

This paper has the primary objective of expanding upon previous experimental analysis by the current authors [8,10] by considering the effects of wall heating in annular flow for a range of system pressures, mass flux and void fraction in a very thin duct. These measurements have been made in a refrigerant fluid, R-134a (SUVA) at elevated temperature and pressure conditions. At 0.9 and 2.4 MPa, R-134a has a liquid-to-vapor density ratio of 27.0 and 7.3 respectively, compared to a ratio of about 850 for atmospheric pressure air-water. Similarly, the surface tension of R-134a is 0.0069 and 0.0021 N/m at 2.4 and 0.9 MPa, respectively, compared with 0.072 N/m for water at atmospheric conditions.

The specific objectives of this paper are to: a) provide detailed local measurements of void fraction, droplet frequency, droplet velocity, and thereby infer distributions of mean droplet diameter and interfacial area concentration using hot film anemometry, b) investigate the effect of wall heating by comparing the results with those of adiabatic flows, and c) investigate the effect of liquid-to-vapor density ratio and surface tension on local phase distributions in both the narrow and wide directions of the cross-section.

Experimental Investigation

The test section shown in Figure 1 has been designed to be flat, thin and rectangular for easy optical access. This high aspect ratio test section and the two-phase flow facility have been described in detail in our previous papers [8-11] and only a brief overview will be provided here. The R-134a facility consists of a chiller, pressurizer, circulating canned rotor pump, CO_2 heat exchanger, loop heaters, various throttle valves and flow meters, and a vertical test section. Loop conditions are established by programmed logic controllers. The test section has a length of 1.2 m, a cross-section aspect ratio (width/thickness) of 22.5, and a hydraulic diameter of 4.85 mm. These test section dimensions facilitate the use of thin, transparent heater films that enable visual observations and are consistent with the flow and control capabilities of the test loop. Optical access to the flow is provided by eight quartz windows, each 38.1 mm thick by 76.2 mm wide by 0.28 m long. The working fluid used in this study is refrigerant R-134a (SUVA) which is of scientific interest because of its very low liquid-to-vapor density ratio and low surface tension.

A unique feature of the test section is the use of heating elements on the inside surfaces of the quartz window, which are comprised of thin transparent films that are rugged enough to provide the required heat input. The areas between the quartz windows contain the brushes to carry current to the window films. The triple-track window heater design consists of three transparent metallic oxide conductive films, vacuum deposited on the inside surface, with an anti-reflective coating on the outside. Three silver epoxy buses deliver the current at both ends of the window, and connect with the silver graphite brushes. The power to each of the three heater films on each window is independently controlled, so various heating profiles can be investigated.

In the present experiments, the two-phase flow field was created by a phase change in the test section due to power addition through the window heater strips. The inlet temperature was

controlled by means of a heater located upstream of the test section inlet. Slightly subcooled R-134a was introduced to the test section and heat was applied uniformly to the six windows comprising the lower three power steps. For experiments conducted for comparison to earlier adiabatic annular flow tests, the window power for a given combination of pressure and mass flow rate was adjusted to produce the same cross-sectional average void fraction at X/L=0.86. The total net heat addition ranged from 2.3 to 9.2 kW. The heat losses were quantified experimentally and generally accounted for less than 10% of the gross energy input.

The instrumentation used in the R-134a experimental program has been extensively discussed in our previous papers [8-11]. Cross-sectional average and line-average void fraction measurements were obtained using a gamma densitometer system (GDS). This instrument features a 9-curie Cesium-137 gamma source and a NaI detector. For each experimental condition, the average void fraction was established by using a wide gamma beam that interrogated the entire duct cross-section at a streamwise position of X/L=0.86. The uncertainty of this measurement ($\pm 2\sigma$) has been determined empirically as ± 0.015 in void fraction.

All of the data profiles reported in this paper were measured using dual-sensor hot-film anemometer (HFA) probes (made of platinum with 25 μm diameter and 254 μm active length), which have been discussed at length in a previous publication [8]. For each sensor pair, the upstream hot-film measurements of the local void fraction are made by quantifying the time the sensor is exposed to the vapor phase relative to the total measurement time. The local interfacial velocity is calculated by dividing the known spacing between the sensors by the mean interface transport time. The latter is obtained directly by taking the cross-correlation between the output voltage signals from the upstream and downstream sensors. Two types of HFA probes were used. One was mounted in a hole in one of the quartz windows to traverse across the narrow (Z)

dimension at X/L=0.74. The other was mounted in an instrument access port between windows 3 and 4 (Figure 1), to traverse the wide (Y) dimension at X/L=0.77. The measurement uncertainties ($\pm 2\sigma$) associated with the HFA probes have been quantified empirically as follows: 0.027 for void fraction, 7.5% for near-wall velocity, and 7% for far-wall velocity.

Measurements of local void fraction, interfacial velocity and frequency were obtained from direct analysis of the HFA output voltage signals. In the region of the two-phase flow comprised solely of dispersed liquid droplets in continuous vapor, these direct measurements were then used to compute the local mean droplet diameter:

$$d_d = 1.5\frac{V_d \alpha_d}{f_d} \tag{1}$$

Ishii and Mishima (12) characterized the average interfacial area concentration in annular flow by combining contributions from interfacial waves and dispersed droplets. If their expression is applied locally in the region of the flow where only the vapor core and droplets are present, the interfacial area density reduces to

$$a_i = \frac{4 f_d}{V_d} \tag{2}$$

Galaup [13] derived the above equation from geometric considerations in bubbly flows where the characteristic size of the bubbles far exceeded the effective size of the measurement volume. In the current experiments, very small droplets (i.e., size of the same order as the 25 μm diameter HFA sensor) were measured. Therefore, it is expected that the largest error associated with the application of eq. (2) will be for very small droplets which generally occur for cases with void fraction in excess of 90%. A detailed discussion of these derived parameters is given in [6, 8].

Results

Detailed local measurements of void fraction, droplet frequency, diameter, velocity, and interfacial area concentration were obtained in wall heated annular refrigerant flow through a narrow duct. The three operating variables are pressure (0.9 to 2.4 MPa), mass flow rate (106 to 532 kg/hr) and cross-sectional average void fraction (0.83 to 0.94). The three system pressures investigated provide liquid-to-vapor density ratios of 7.0 to 27.0. For some of the experiments, the inlet flow was heated to produce adiabatic conditions in the test section, and to reproduce the same average void fraction obtained at the same location during similar wall-heated test runs. The HFA voltage scans were used only when the signal quality was considered adequate for accurate determination of local void fraction. For some flow conditions, in particular at high flow rates, it was difficult to define a threshold, therefore, droplet frequency and diameter measurements could not be made. However, the time-averaged interfacial velocity could be obtained using the dual-sensor HFA probe (via cross-correlation) even for the highest flow rate. For all experimental runs, the cross-sectional average void fraction ($\overline{\alpha}$) was established at $X = 1.03$ m using the wide beam gamma densitometer edge measurement.

The local void fraction profiles for the heated case are presented first in Figures 2a, 2b, and 2c for each mass flow rate of 106, 266 and 532 kg/hr, and compared with the corresponding adiabatic cases. For all flow rates, at high void fractions, the behavior of these profiles for the two types of heating is similar. There is an inversion in the void fraction profiles, as the wall-bounded film thickness decreases. The decrease in the void fraction in the center of the test section is due to the concentration of droplets emanating from the test section edge liquid film. This fact is corroborated by the interfacial area concentration profiles in Figure 3 which show an increase in droplet concentration toward the center of the test section at high pressures. Although there is no significant difference in the overall trend displayed in the two types of heating for the same flow conditions, near-wall measurements are seen to differ. At the center, the magnitude of the dip is

higher in the case of heated flow for low rates (Figure 3a). Therefore, local measurements in heated flows are important for model and code validation. Having discussed the fundamental similarities and differences in adiabatic and wall-heated annular flows, further discussions will be restricted to wall-heated annular flows.

The basic structure of the phase distribution in the narrow Z-dimension is dependent on the system pressure, which is shown in Figure 4. For w=532 kg/hr and α=0.71, as the pressure is increased from 0.9 MPa to 2.4 MPa, the flow goes through several distinct transitions in the two-phase flow structure. This average void fraction was chosen so that for some conditions, a churn-turbulent flow would be produced using the window heaters. It is clear from this figure that at lower pressures of 0.9 MPa and 1.6 MPa, the void fraction profile attains the classic parabolic shape characteristic of the transition flow regime. As the pressure is increased to 2.1 MPa, the film thickness decreases on the wall, as the void profile becomes flat. At the highest pressure of 2.4 MPa (equivalent to 13.7 MPa in steam-water with the same liquid-to-vapor density ratio as the refrigerant in this study), the profile becomes inverted, with maximum void fraction near the wall and minimum void fraction at the duct centerline. This trend, also observed in earlier adiabatic experiments, may be explained as follows.

The strong inversion in the void fraction profiles in the narrow Z-dimension is caused by two mechanisms: 1) increasing the system pressure thins the liquid film on the walls, redistributes the liquid to the edges where the disturbance waves with larger amplitudes form over a thicker base film; 2) the disturbance waves are sheared off by the fast-moving vapor, entraining larger diameter droplets into the vapor core. The second mechanism, in conjunction with a much lower surface tension (At 2.4 MPa, R-134a has a surface tension which is significantly lower than that of water at any pressure), increases the Weber number. As the Weber number increases, the entrainment fraction increases. This phenomenon is evident from Figure 5 which shows the void fraction distribution in both dimensions at 0.9 and 2.4 MPa for an average void fraction of 0.83 and flow rate of 266 kg/hr. As mentioned previously, the Z and Y dimension void fraction profiles were measured with HFA probes at streamwise positions of X/L=0.74 and 0.77, respectively. So

although the X positions of the two data scans in each figure are not the same, the cross-sectional average void fraction varied little over this interval. At low pressure, the void fraction is fairly uniform across most of the duct in both the narrow and width dimensions, and quickly tapers close to the walls and the edges. The near-wall gradient is especially confined within a region extending to only about 2 to 3 mm from the unheated transverse edges of the test section where the void fraction reaches a local minimum of nearly 0.4. When the pressure is increased to 2.4 MPa for the same flow rate and average void fraction, the narrow dimension profile inverts with the dip in the vapor core. The width dimension profile stays flat as it does for the lower pressure in the vapor core, however, the void fraction shows a steady decrement much farther than 2 to 3 mm from the edges. This suggests the presence of thicker liquid films at the edges and disturbance waves with large amplitudes. This phenomenon appears to be characteristic of flows in high pressure systems in high aspect ratio ducts.

Plots of void fraction, droplet frequency, droplet diameter and droplet interfacial area density are shown in Figures 6 through 9 for different flow rates. Profiles are given for two pressures and where available, for three pressures. If reliable droplet frequency measurements could be made, interfacial area density profiles could be made available through the simple relationship, $a_i=4f_d/V_d$, since droplet velocity measurements obtained from cross-correlation has always been reliable. However, the droplet diameter calculation requires frequency, velocity and droplet fraction. For certain pressures in certain regions of the flow, the void fraction, α, is close to 1.0, and the diameter calculation performed using the droplet fraction, $(1-\alpha)$, would contain unacceptable uncertainty. For this reason, droplet diameter profiles are not plotted for certain flow conditions, and certain regions of the flow field.

As shown in Figure 6, high pressure causes a void dip in the center of the test section. This dip is more profound for 266 kg/hr at a slightly lower average void fraction of 0.83. The lower the void and pressure, the more parabolic is the void profile. At the highest flow rate of 532 kg/hr, the trend continues such that the void fraction is lower near the wall for the low pressure, but a small region of void inversion exists near the center for both pressures.

The droplet frequency profiles given in Figure 7 indicate the droplet concentration flux, and provide insight regarding the possible source of these droplets. For the low flow of 106 kg/hr, the frequency profile for the low pressure has a slight decreasing trend toward the vapor core since most of the entrainment occurs at the flat side film. As the pressure is increased to 2.4 MPa, a complete opposite trend is seen where the frequency increases towards the core. Since the void fraction profile for this case is seen to have a slight inversion, it is reasonable to conjecture that the edge film for the higher pressure is much thicker with large amplitude waves than that at low pressure. When these waves are sheared off, larger diameter droplets emanate from the edges. This increasing trend in the frequency from the wall toward the vapor core is also seen for the highest flow of 532 kg/hr at both low and high void fractions of 0.71 and 0.88 (Figure 7c and 7d). For this flow, the increasing trend can be noticed at both pressures. At α=0.71, the flow has not reached a pure annular flow regime. It is probably in its late stage of transition as seen by the asymmetric distribution in droplet frequency (Figure 7c) as well as in void fraction (Figure 6c). At 266 kg/hr (Figure 7b), the frequency profile is flat at the two pressures and void fractions. All the cases clearly show that the droplet concentration increases with increasing pressure.

The interfacial area density (Figure 8) is calculated directly from droplet frequency and droplet velocity measurements. Because the velocity profiles in the droplet field are generally flat as reported previously [6], the trend in the interfacial area closely mimics the measured frequency. To the authors' knowledge, no average or local measurements of interfacial area are available in the literature for heated flow at elevated pressures. The local interfacial area density increases with pressure for almost all flows as seen in the frequency profiles. For a constant void fraction of approximately 0.9 (Figures 8a, 8b and 8d) for P=2.4 MPa, the average interfacial area density increases as the flow rate increases. For the same flow rate and pressure, the interfacial area density is higher for lower void fractions due to the increased droplet frequency. These trends are expected, but the surprising result is that the magnitude of the interfacial area density is significantly higher than the values reported for the air-water flows. The largest interfacial area density reported for air-water flow was 25 cm^{-1} measured at a gas superficial velocity of 37 m/sec

[14] in circular tubes. For a measured droplet velocity field of approximately 6 m/sec, the interfacial area density reported here exceeds 25 cm^{-1} at 532 kg/hr. It may be suggested that the combination of high pressure and a thin non-circular geometry contributed to a large frequency of droplets, thereby increasing the interfacial area compared to air-water flows at atmospheric pressure.

The droplet diameter profiles shown in Figure 9 are another set of inferred measurements, but are significantly more difficult to obtain than interfacial area density. The uncertainty is higher at very high void fractions, since the calculation involves the volume fraction of the droplets. The droplet field features a wide range of droplets from 25 μm to 400 μm, and generally displays an increasing trend in diameter from the wall to the vapor core. For high void fraction flows, the wall film is too small to contribute to large droplets. These large droplets are generated from another source, possibly the thicker edge film. The available droplet diameter profiles do not show any variation in trend as the flow rate or void fraction increases. The diameters vary only between 200 μm and 400 μm in the core of the flow ($0.2 \leq Z/t \leq 0.8$) for all the cases, whereas the droplet frequencies can vary 10-fold (Figure 7). This suggests that the increase in interfacial area density should be attributed more to the increase in droplet frequency than the droplet diameter.

Finally, the droplet velocities measured by the cross-correlation of the two HFA sensors are plotted for three flow rates both in the thickness (Z) dimension (Figure 10) and width (Y) dimension (Figure 11). Table 1 summarizes the flow conditions and the calculated averaged liquid and vapor velocities. It also includes the wave velocity calculated for a neutrally stable film from a simple force balance at the interface between the liquid film and the vapor core yielding,

$$V_w = \frac{\sqrt{\frac{\rho_g}{\rho_l}} V_g + V_l}{1 + \sqrt{\frac{\rho_g}{\rho_l}}}. \qquad (3)$$

Table 1: Flow conditions for Figures 10 and 11

Pressure MPa	$\frac{\rho_g}{\rho_l}$	w kg/hr	Quality, x	Void Fraction, α	V_l	V_g	V_w
0.9	.037	106	.73	.94	.78	3.65	1.24
2.4	.136	106	.68	.94	1.14	1.15	1.15
0.9	.037	266	.33	.83	1.73	4.52	2.18
2.4	.136	266	.44	.83	1.76	2.08	1.84
1.4	.062	532	.46	.88	4.17	7.85	4.9
2.4	.136	532	.60	.88	3.54	5.33	4.02

The average values of vapor velocity, V_g, and liquid velocity, V_l, can be calculated using the one-dimensional relationship in terms of the measured quality and mass flux as

$$V_g = \frac{x}{\alpha}\frac{G}{\rho_g}\,;\; V_l = \frac{(1-x)}{(1-\alpha)}\frac{G}{\rho_l}. \tag{4}$$

The profiles for lower flow rates and a low pressure of 0.9 MPa in Figure 10 offer dramatic evidence of the presence of disturbance waves on the wall. At Z/t<0.2, the droplet velocity is low and follows closely the average liquid velocity (Table 1). Within this region, the velocity increases from this average liquid velocity to the wave velocity, and at Z/t~0.2, jumps to a much higher velocity closely following vapor velocity. It is interesting that although at Z/t<0.2, the droplet frequency and diameter have a higher uncertainty and are difficult to measure, the droplet velocities through the cross-correlation are reliable and follow theoretical averaged velocities. It is conjectured that the measurements made close to the wall are measurements of liquid ligaments and/or large droplets and HFA is generally more biased towards bigger droplets.

The high pressure profiles provided both in Figure 10 and 11 are flat since the average liquid and vapor velocities for these conditions are closer to each other in magnitude. This is the uniqueness of the high pressure systems where annular flow is possible even for low vapor

velocities close to 1 m/sec, whereas in air-water systems such low velocities are not possible in separated annular flows. The transverse profiles in Figure 11 have a profound dip in the middle of the test section for lower pressures. Flow visualization displayed half-waves extending from one edge to the middle of the test section. These waves subsequently coalesce with half-waves from the other edge, causing a dip in the middle. In this region, the velocities are generally low because of the agglomeration of large droplets as was seen in the droplet diameter profiles at 2.4 MPa in Figure 9.

Summary and Conclusions

An experimental study has been conducted to acquire local measurements of void fraction, interfacial velocity and droplet frequency in flows of R134a through a vertical, high aspect ratio rectangular duct. These measurements were used to infer the local droplet size and interfacial area concentration. By considering the effect of wall heating, the results presented in this paper expand the database for annular flows in a rectangular geometry. By applying electrical power to thin, transparent metal oxide heaters on the inside surfaces of quartz windows, vapor was generated at the walls to create annular flow in the test section from a subcooled inlet. A comparison between the local phase distributions in heated flows to those obtained in earlier adiabatic experiments show generally close agreement, but there are some differences in the near-wall region, particularly for average void fractions at the lower limit of the annular flow regime.

As described in previous papers [8-11], the unique characteristic of R134a is that the liquid-to-vapor density ratio can be reduced by two orders of magnitude, and surface tension by an order of magnitude compared to water at atmospheric conditions. Acquisition of local two-phase flow data under these conditions has shed light on many heretofore unreported physical phenomena. Perhaps the most important of these phenomena is the manner in which the liquid phase is redistributed when the system pressure is increased, i.e., reducing the difference in density between the liquid and vapor phases and the surface tension. These property effects increase the

Weber number at high pressures, thereby increasing the droplet entrainment from the edges. To fully ascertain this effect, a new hot-film anemometry device was installed to enable acquisition of local void fraction along both test section dimensions in the horizontal plane. Two-dimensional plots of local void fraction clearly demonstrate that at high pressure, the liquid is redistributed from the wide duct walls toward the edges of the test section. Incrementally increasing the pressure from 0.9 to 2.4 MPa shows a transition from a classic parabolic vapor phase distribution to one that has its maximum near the heated wall.

Pressure effects are also evident in the distributions of interfacial velocity. For data scans across the narrow (Z) dimension, the high pressure data show a small monotonic increase in velocity from the duct wall to the center of the test section, suggesting that the sensing probe is exposed only to the dispersed droplet field. At lower pressures, the velocity profile displays a clear transition from the near-wall region, where the HFA probe likely senses the interface between continuous liquid and dispersed bubbles in the wall-bounded liquid film. At the center of the test section, the local velocity is much higher, since the sensor measured predominantly the dispersed liquid droplets in the continuous vapor core. Between these two regions, the probe appears to measure the waves in the liquid film, based upon a comparison to a simple force balance derivation of a neutrally stable film.

Acknowledgements

The authors gratefully acknowledge Messrs. W.O. Morris and L. Jandzio for their efforts in the operation of the test facility, and Dr. G.J. Kirouac for his direction of the experimental program. Special thanks are due to Mr. S.W. D'Amico who contributed to the development of the hot-film anemometer probe traversing and data acquisition systems.

References

1. Hewitt, G.F. and Hall-Taylor, N.S. (1970) *Annular Two-Phase Flow*, Pergamon Press.
2. Azzopardi, B.J. (1997) "Drops in Annular Two-Phase Flow," *Int. J. Multiphase Flow*, Vol. 23, Suppl., pp. 1-53.
3. Henstock, W.H. and Hanratty, T.J. (1976) "The Interfacial Drag and Height of the Wall Layer in Annular Flow," *AIChE. J.*, Vol. 22, pp. 990-1000.
4. Tatterson, D.F., Dallman, J.C. and Hanratty, T.J. (1977) "Drop Sizes in Annular Gas-Liquid Flows, *AIChE J.*, Vol. 23, pp. 68-76.
5. Hanratty, T.J. and Dykhno, L.A. (1997) "Physical Issues in Analyzing Gas-Liquid Annular Flow," *Exp. Heat Transfer Fluid Mech. Thermodyn.* Ed. ETS, Vol. 2, pp. 1127-1136.
6. Kataoka, I. and Ishii, M. (1982) "Mechanism and Correlation of Droplet Entrainment and Deposition in Annular Two-Phase Flow," Argonne National Laboratory Report ANL-82-44.
7. Kataoka, I. and Serizawa, A. (1990) "Interfacial Area Concentration in Bubbly Flow," *Nuclear Engineering and Design*, Vol. 120, pp. 163-180.
8. Trabold, T.A., Kumar, R. and Vassallo, P.F. (1999) "Experimental Study of Dispersed Droplets in High-Pressure Annular Flow," *J. Heat Transfer*, Vol. 121, pp. 924-933.
9. Trabold, T.A. and Kumar, R. (2000a) "Vapor Core Turbulence in Annular Two-Phase Flow," *Experiments in Fluids*, Vol. 28, pp. 187-194.
10. Trabold, T.A. and Kumar, R. (2000b) "High Pressure Annular Two-Phase Flow in a Narrow Duct. Part I: Local Measurements in the Droplet Field," *J. Fluids Eng.*, Vol. 122, pp. 364-374.
11. Kumar, R. and Trabold, T.A. (2000) "High Pressure Annular Two-Phase Flow in a Narrow Duct. Part II: Three-Field Modeling," *J. Fluids Eng.*, Vol. 122, pp. 375-384.
12. Ishii, M. and Mishima, K. (1981) "Study of Two-Fluid Model and Interfacial Area," Argonne National Laboratory Report ANL-80-111.
13. Galaup, J.P. (1976) "Contribution to the Study of Methods for Measuring Two-Phase Flow," Centre D'Etudes Nucleaires de Grenoble, Report No. 136.
14. Wales, C.E. (1966) "Physical and Chemical Absorption in Two-Phase Annular and Dispersed Horizontal Flow," *AIChE Journal*, Vol. 12, pp. 1166-1171.

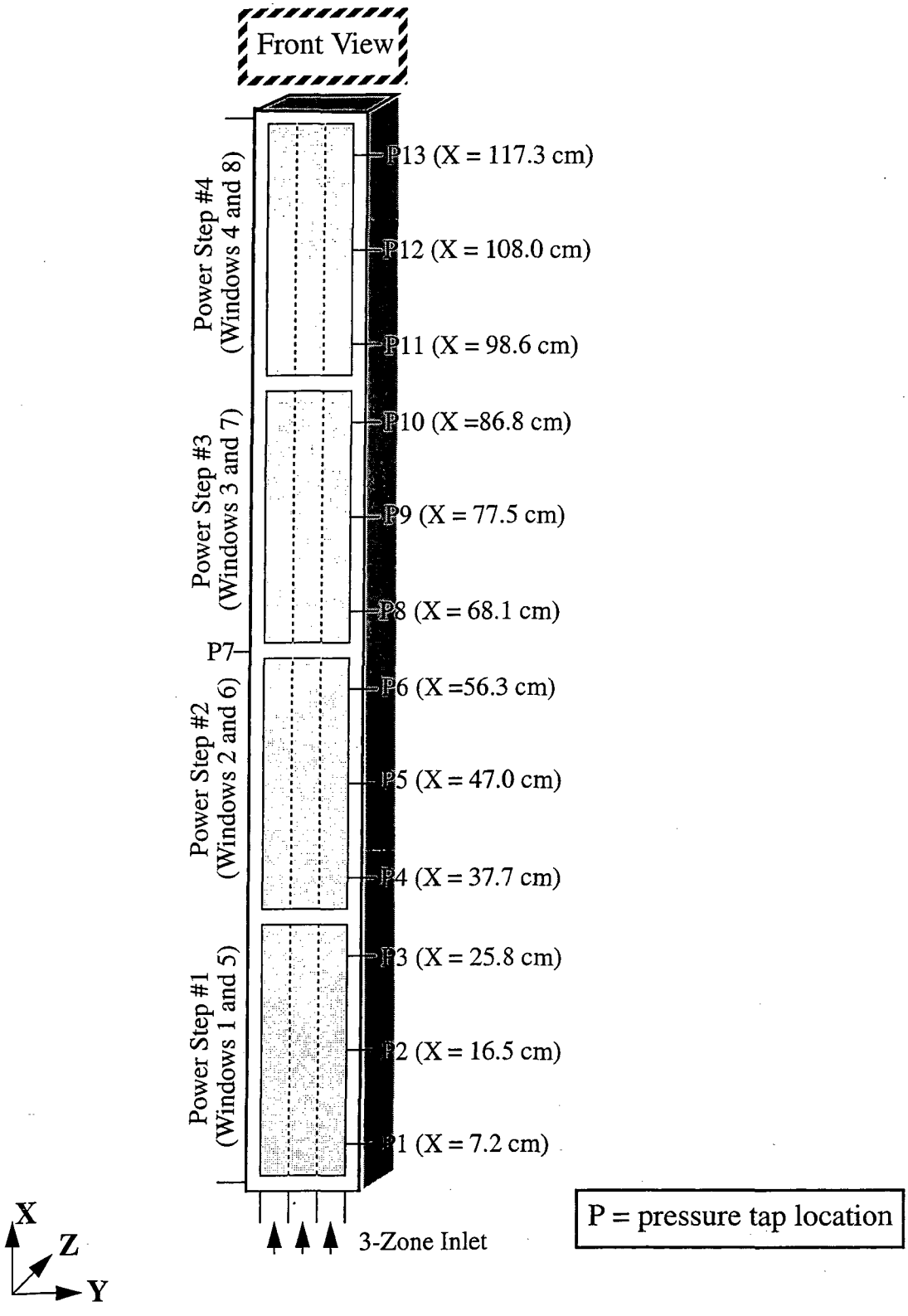

Figure 1: Test Section and Measurement Locations

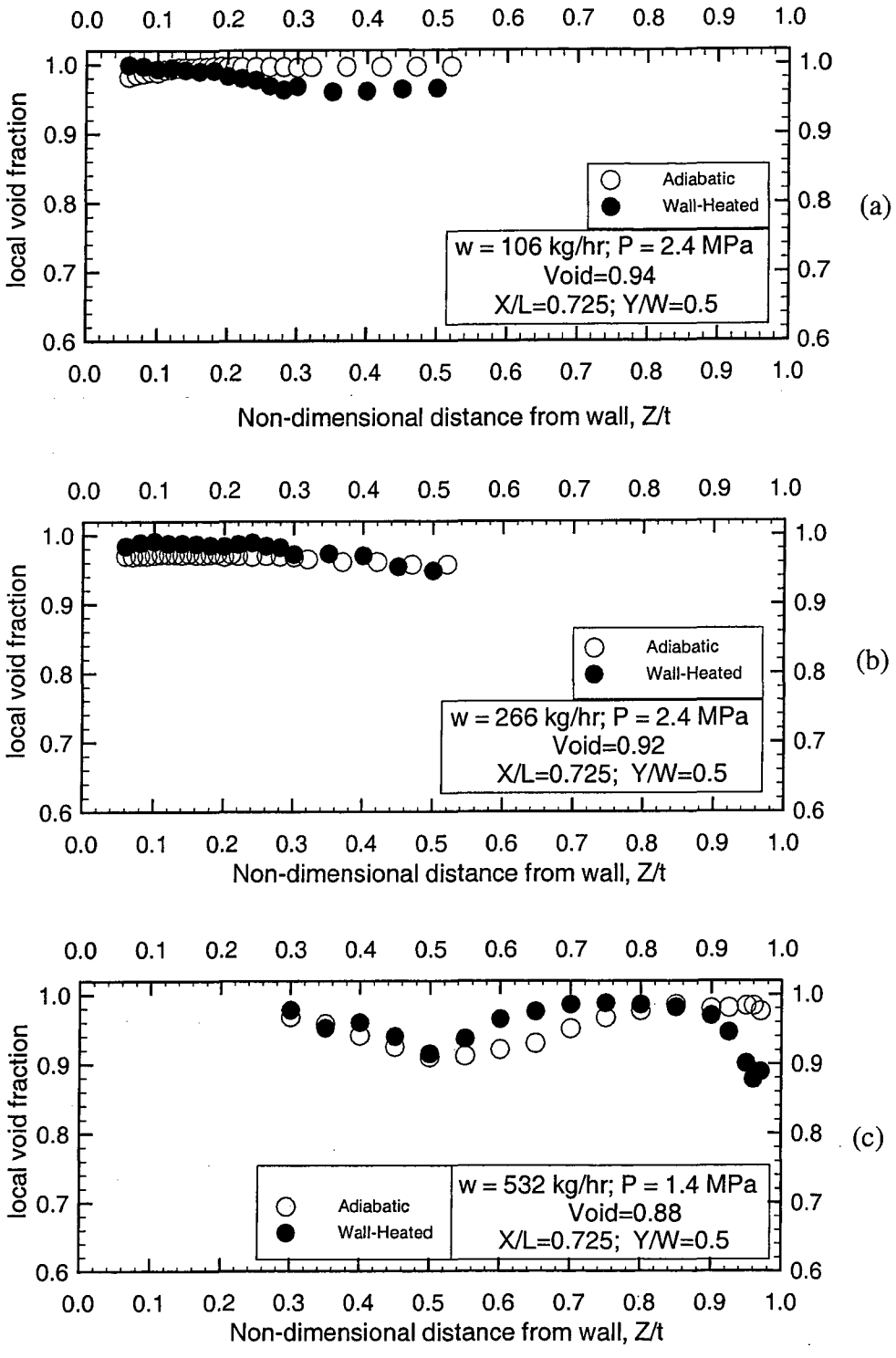

Figure 2: Comparison of Thickness Dimension Void Fraction Scans Between Adiabatic and Wall-Heated Cases

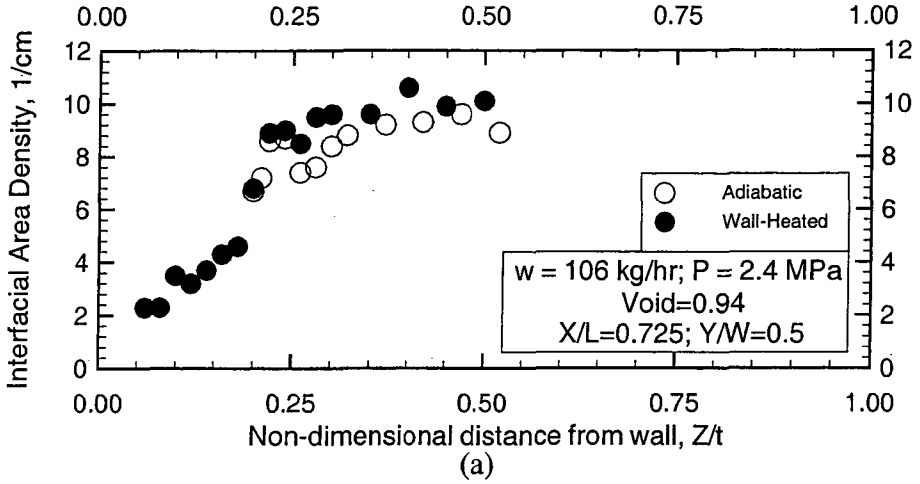

(a)

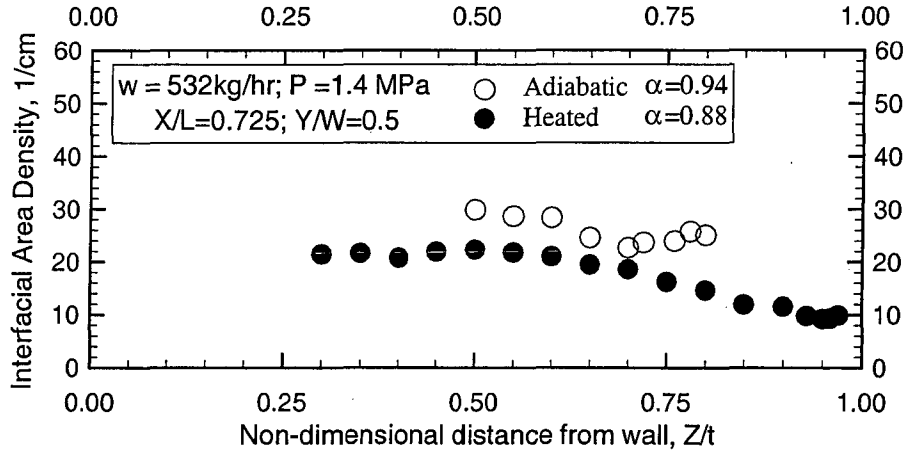

(b)

Figure 3: Comparison of Thickness Dimension Interfacial Area Density Profiles Between Adiabatic and Wall-Heated Cases

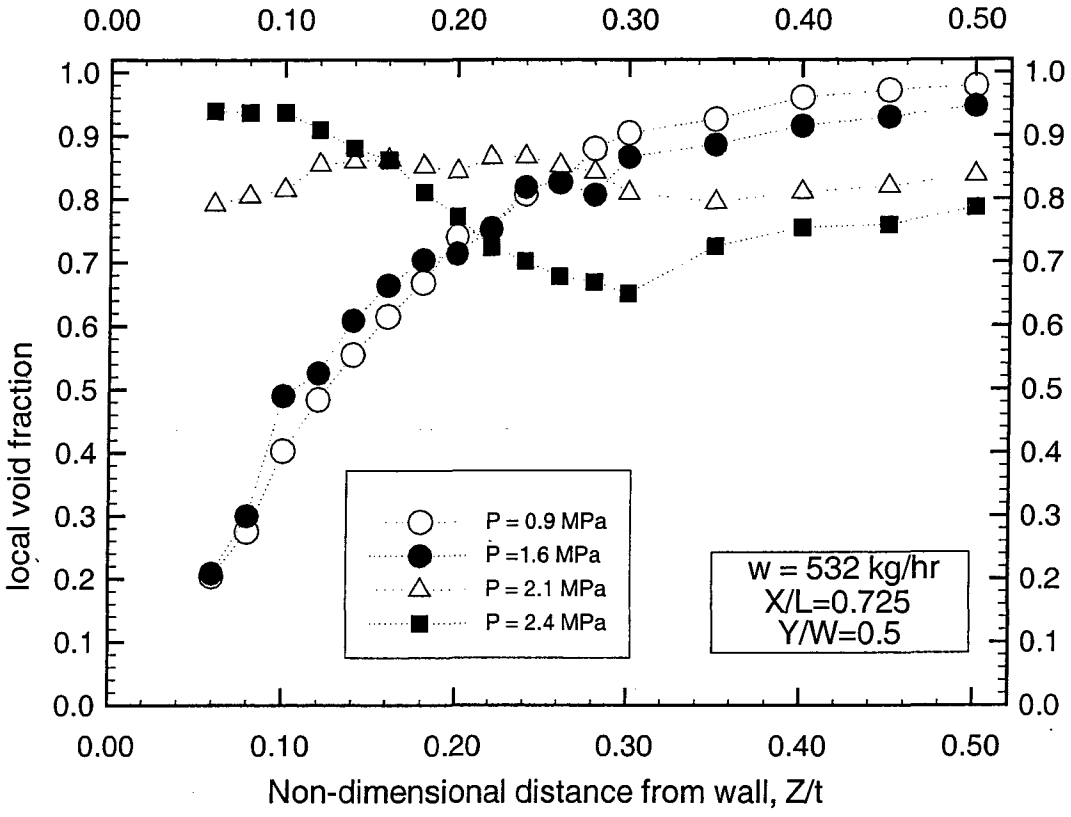

Figure 4: Effect of Pressure on Void Fraction Scans in the Thickness Dimension for w = 532 kg/hr and α=0.71

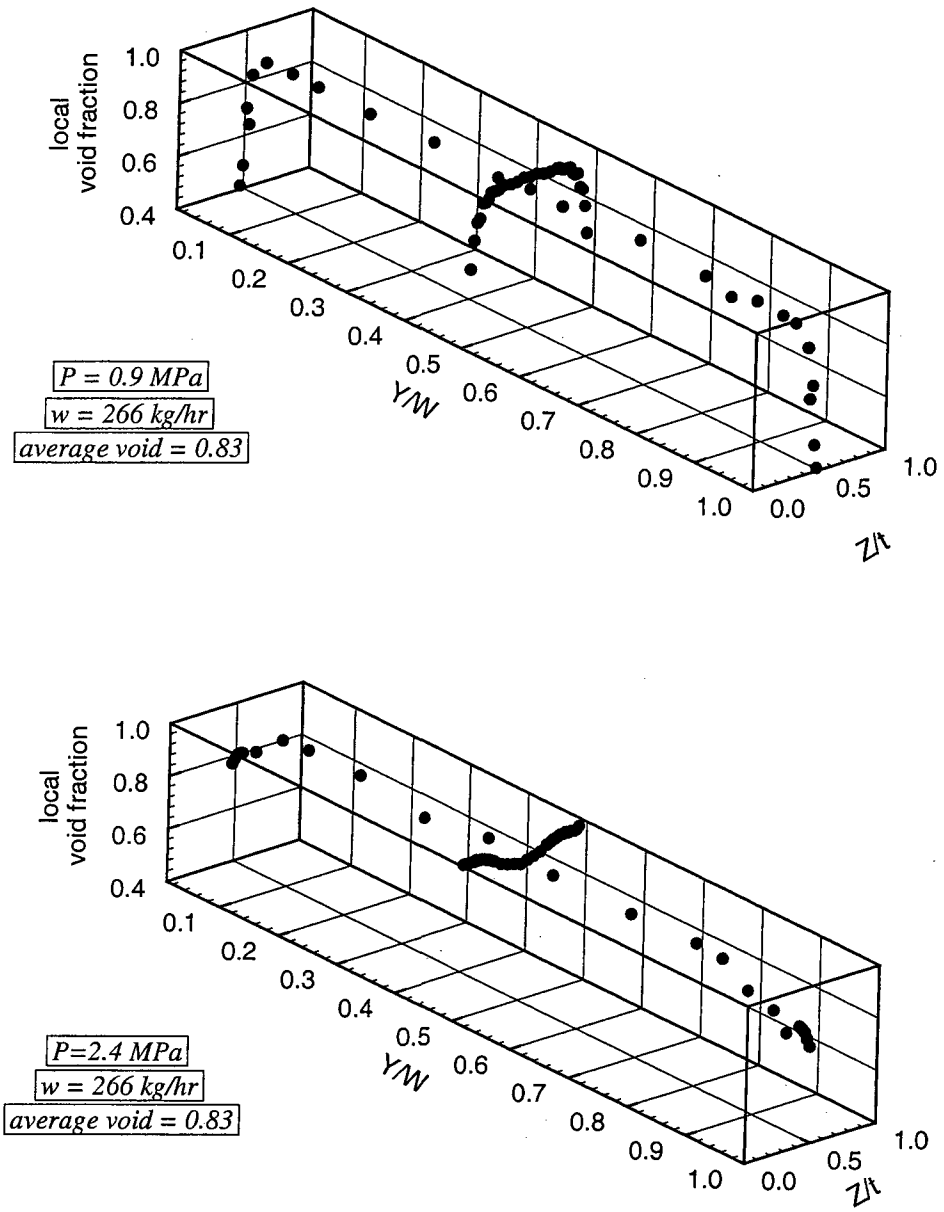

Figure 5: Void distribution in the narrow and width dimensions at two different pressures.

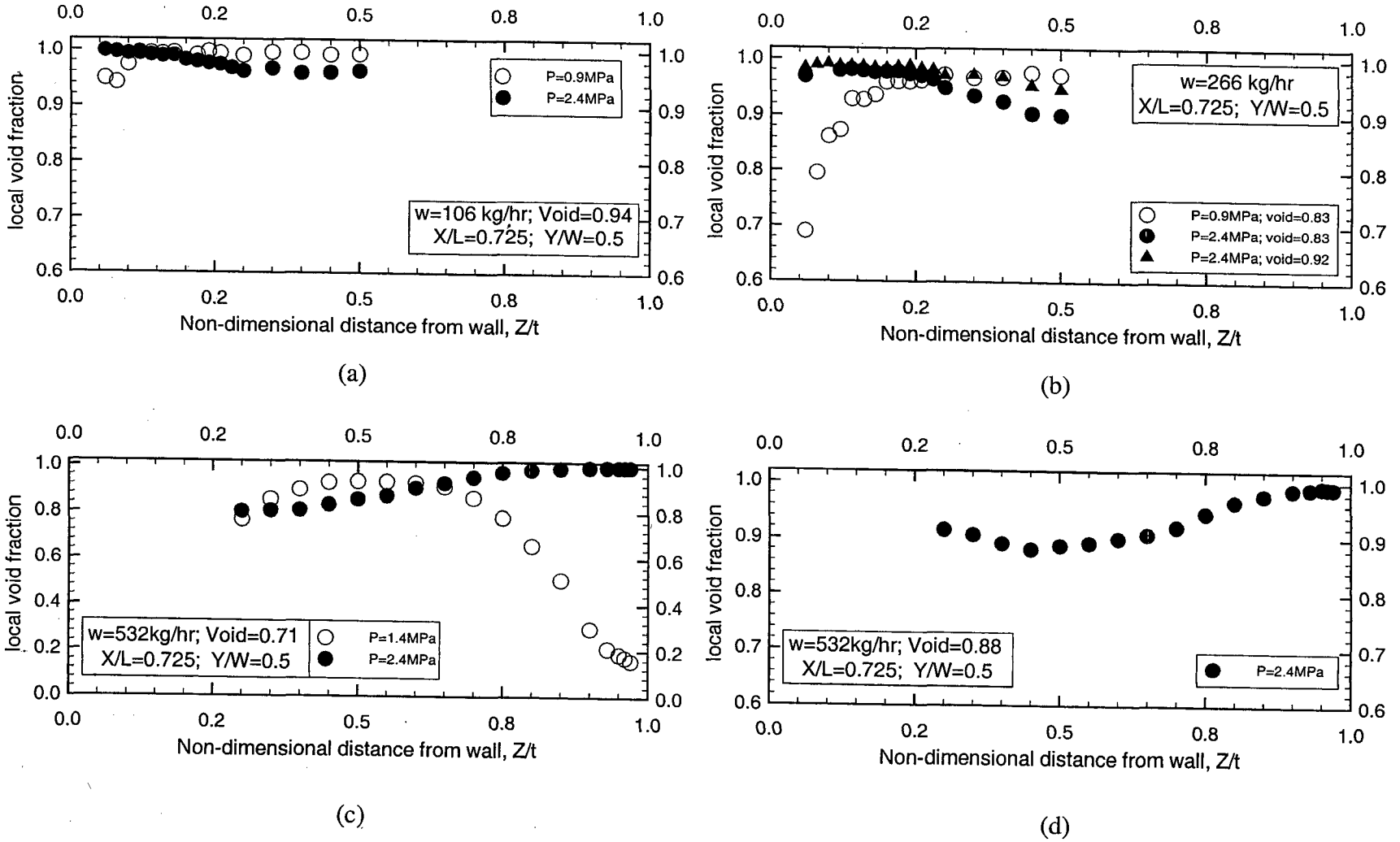

Figure 6: Effect of Pressure on Thickness Dimension Profiles of Void Fraction at Different Flow Rates

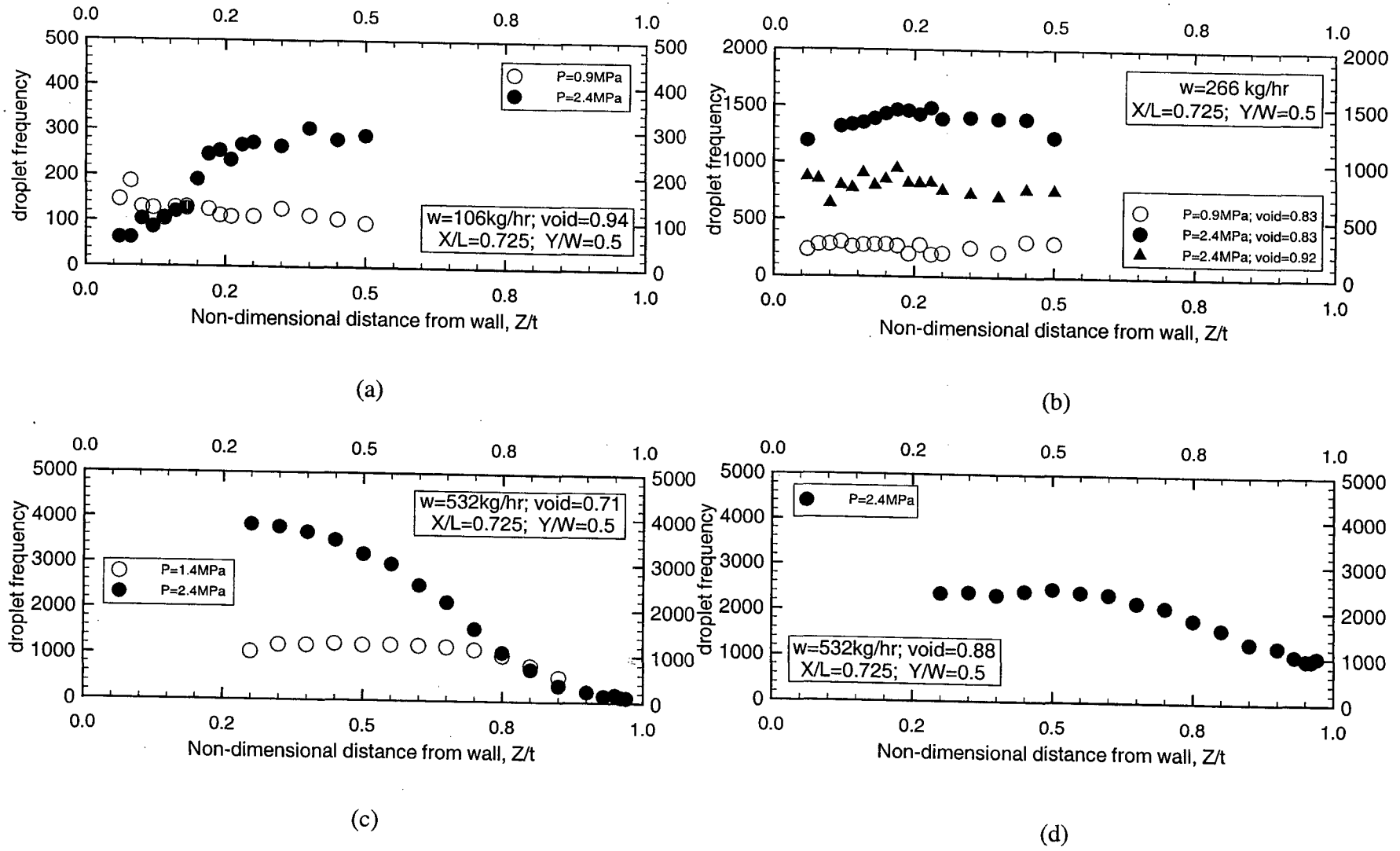

Figure 7: Effect of Pressure on Thickness Dimension Profiles of Droplet Frequency

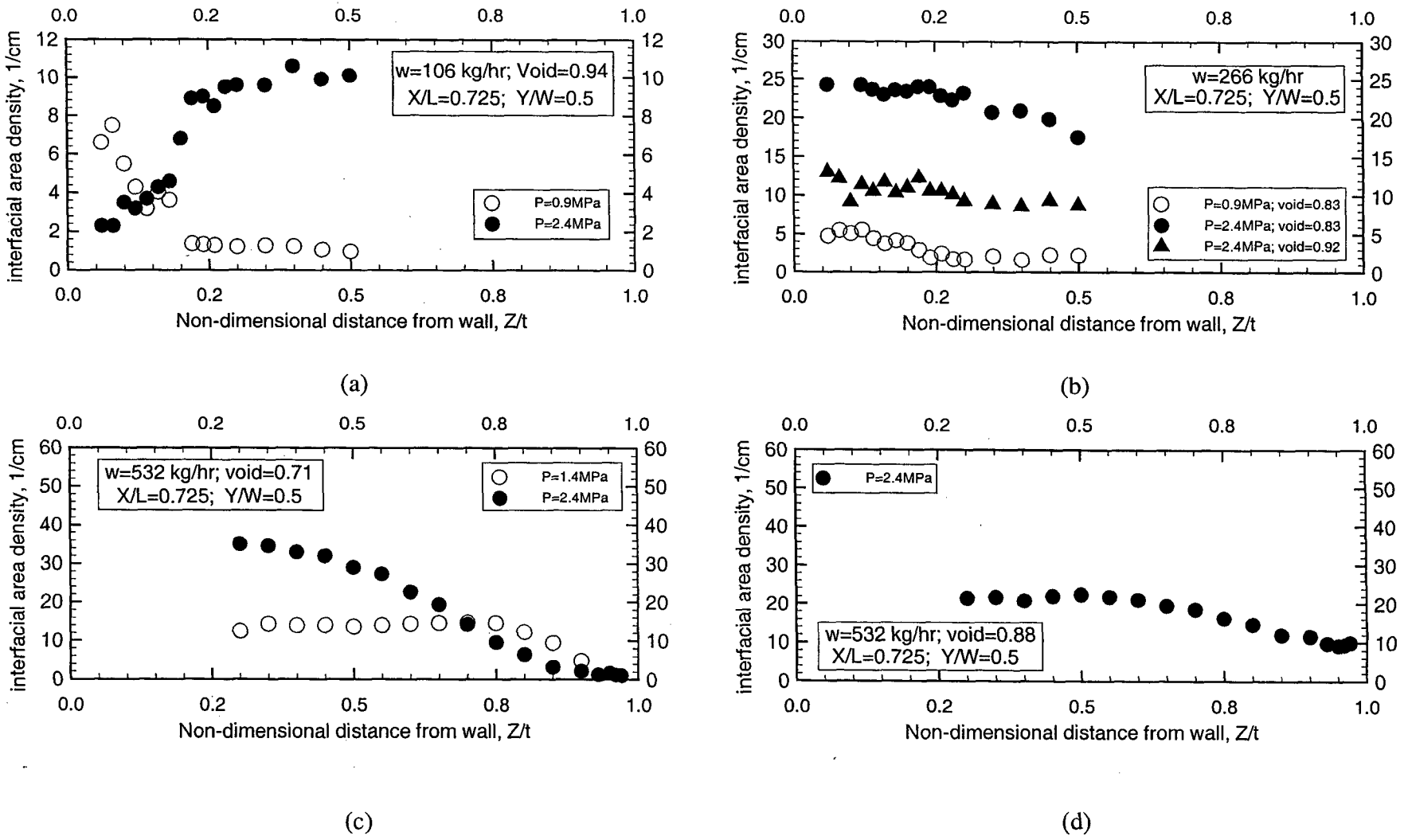

Figure 8: Effect of Pressure on Thickness Dimension Profiles of Interfacial Area Density at Different Flow Rates

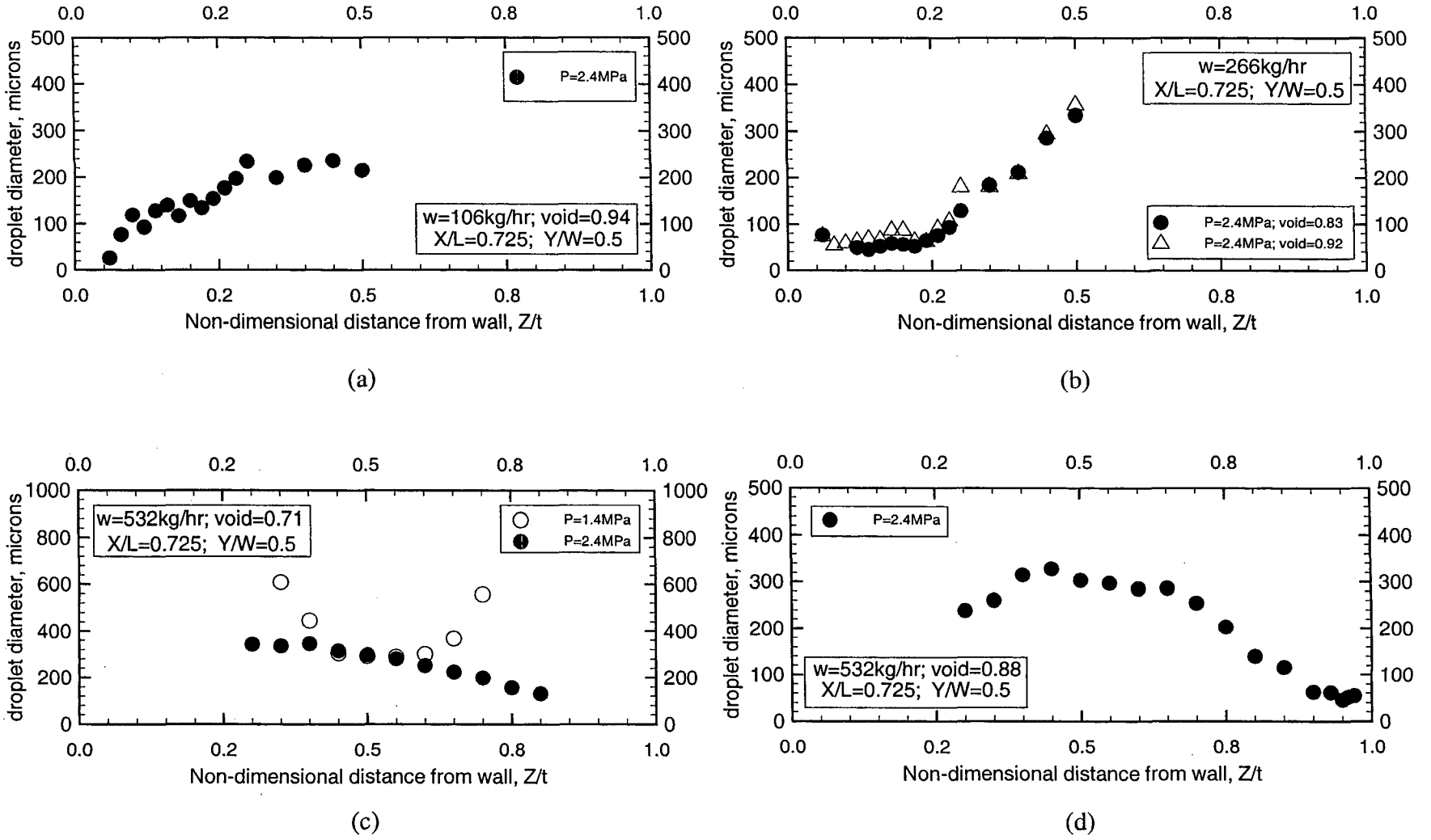

Figure 9: Effect of Pressure on Thickness Dimension Profiles of Droplet Diameter

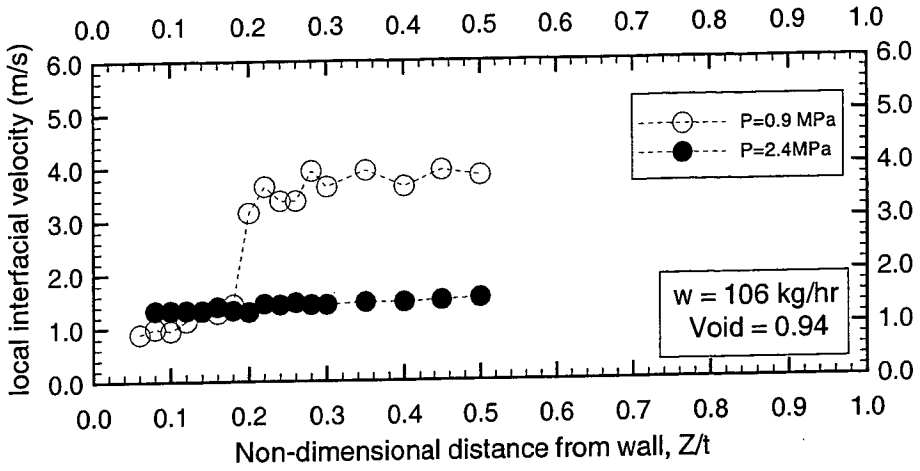

(a)

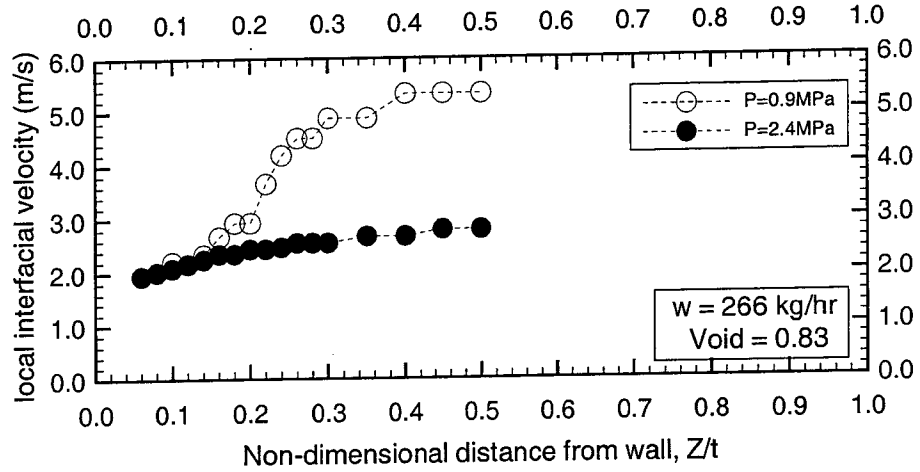

(b)

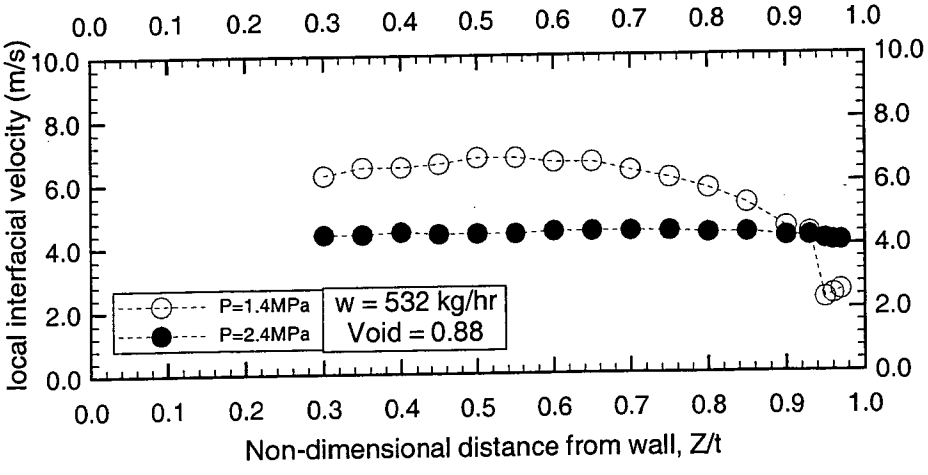

(c)

Figure 10: Effect of Pressure on Thickness Dimension Interfacial Velocity Profiles

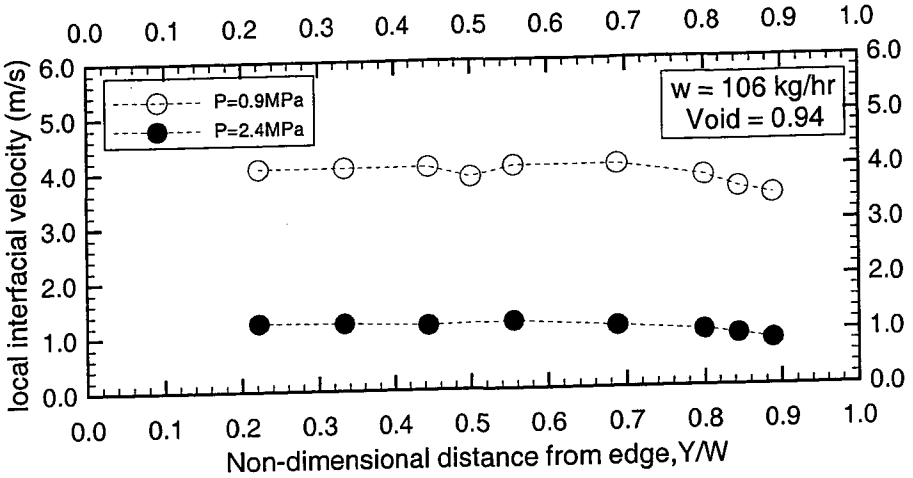

(a)

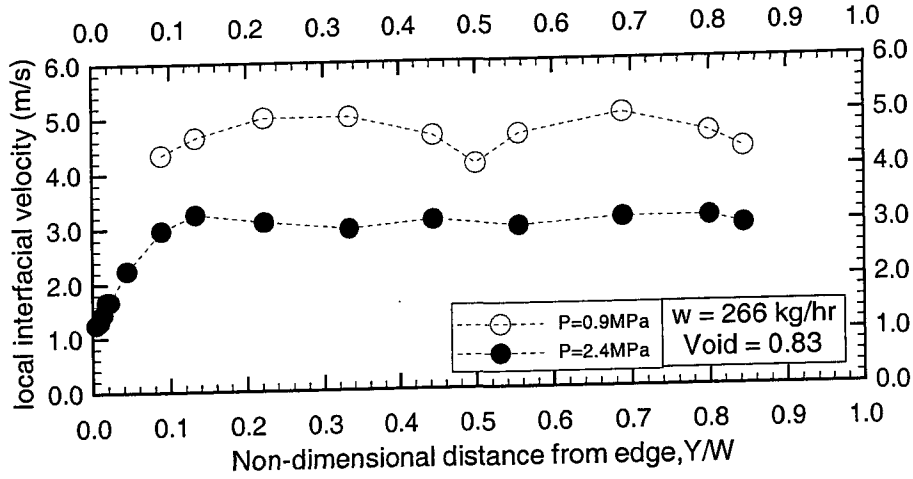

(b)

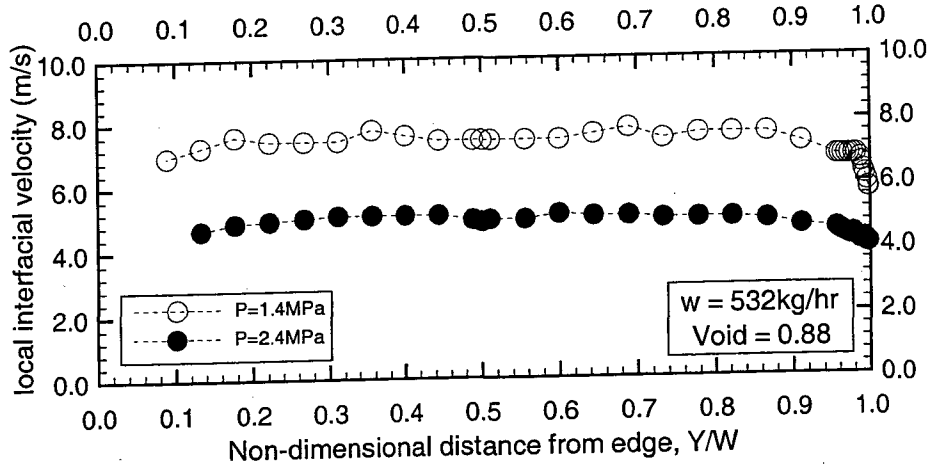

(c)

Figure 11: Effect of Pressure on Width Dimension Interfacial Velocity Profiles